Relationship between sound radiations resulting from airborne-sound and point-force excitations of a double-leaf infinite elastic plate

Yairi, Motoki
Sakagami, Kimihiro
Okuzono, Takeshi

(Citation)
Acoustical Science and Technology,40(5):325-335

(Issue Date)
2019-09-01

(Resource Type)
journal article

(Version)
Version of Record

Acoust. Sci. & Tech. **40**, 5 (2019)

PAPER

Relationship between sound radiations resulting from airborne-sound and point-force excitations of a double-leaf infinite elastic plate

Motoki Yairi[1,*], Kimihiro Sakagami[2] and Takeshi Okuzono[2]

[1]*Kajima Technical Research Institute, Chofu, Tokyo, 182–0036 Japan*
[2]*Environmental Acoustics Laboratory, Department of Architecture, Graduate School of Engineering, Kobe University, Rokko, Nada, Kobe, 657–8501 Japan*

(*Received 14 November 2018, Accepted for publication 20 May 2019*)

Abstract: This paper presents an expanded theory for relating airborne-sound-excited and force-excited sound radiations from solid structures. Although the reduction of these two types of sound radiation is a fundamental issue in noise-control engineering, each of them has been historically treated as a separate issue. The reduction in the former is normally called airborne sound insulation and separated from the latter, especially in architectural acoustics. A previous study (M. Yairi *et al.*, *J. Acoust. Soc. Am.*, **140**, 453–460 (2016)) established a fundamental relationship between the sound radiations from random-incidence sound-excited and point-force-excited vibrations of a single-leaf infinite elastic plate. A conversion function that relates the two excitation cases was presented in a simple closed form, not including the parameters of the plates, which included of only the specific impedance and the acoustic wavenumber of the medium surrounding the plate. In this paper, the applicability of the conversion function is expanded from a single-leaf infinite elastic plate model to a double-leaf infinite elastic plate model. The sound radiation from a double-leaf infinite elastic plate driven by random-incidence sound and that driven by point-force excitation are theoretically investigated. The conversion function derived from the present model successfully relates the two excitation problems at all analyzed frequencies and has been shown to agree with the previously established single-leaf theory.

Keywords: Random-incidence sound, Point-force excitation, Double-leaf infinite elastic plate, Conversion function

PACS number: 43.55.Rg, 43.40.Rj, 43.55.Ti [doi:10.1250/ast.40.325]

1. INTRODUCTION

1.1. Background

Sound radiation from vibrating solid surfaces is generally caused by either airborne-sound- or force-excited vibration. The reduction of these two types of sound radiation is a fundamental issue in noise-control engineering and a basic requirement for many buildings, cars, ships and airplanes to realize a comfortable acoustic environment [1,2].

In architectural acoustics, sound radiation due to the airborne-sound-induced vibration of walls, floors and other solid boundaries between rooms is normally called airborne sound transmission. The study of airborne sound transmission has historically been separated from that of sound radiation due to the force-excited vibration of solid structures [3]. The insulation performance in terms of airborne sound transmission is typically evaluated under the assumption of random-incidence sound since various incidence angles are likely to occur in actual situations. Considering the recent increase in the number of collective housing units in urban areas, the demand for higher-performance airborne sound insulation is growing. Double-leaf structures with air gaps between leaves, such as double-leaf walls, double-leaf floors and double-leaf ceilings, generally have a higher insulation performance than single-leaf alternatives. Therefore, many researchers have carried out analytical and experimental studies on double-leaf structures. In recent years, practical models have been proposed to predict commonly used double-leaf walls considering the effects of layered panel bending stiffnesses [4], structure-borne sound transmissions via connections, and sound absorption in cavities [5,6]. Three-dimensional finite element acoustic models have also been developed to predict the sound reduction index of double-leaf walls [7].

*e-mail: yairi@kajima.com

The reduction sound radiation from force-excited vibration is also a fundamental issue in architectural acoustics. Several sources of excitation force contribute to sound radiation from the surfaces in buildings, such as building facilities, railways and road traffic vibrations [1,2]. Double-leaf structures are also suitable for the reduction of sound radiation from these types of force-excited vibration. To reduce the force-excited sound radiation from a double-leaf structure, practical methods using porous layers in the cavity [8] and perforated board in combination with honeycomb layer systems [9] have been theoretically studied. Floor impact sound problems, such as footfall, are another typical source of force-excited sound radiation. Practical models have been developed to predict the impact sound insulation of double-leaf floors including floating floors [10,11]. In most analyses of sound radiation from force-excited vibration, the radiation and vibration characteristics of the structures are generally investigated assuming a point and/or distributed excitation force as the external force(s) in underwater acoustics [12] as well as architectural acoustics.

As described above, airborne sound transmission through solid boundaries and sound radiation from force-excited vibrating surfaces have historically been treated as two separate issues in architectural acoustics because of the different sources of external force. There have only been a few studies on the relationship between the floor impact sound level and the floor's sound transmission loss [13,14]. Sound radiations from airborne-sound-induced and force-excited vibrations are, however, similar phenomena in terms of their radiation from vibrating bodies. The coincidence effect of walls is not a phenomenon peculiar to either excitation source. Additionally, the mass-air-mass resonance of double-leaf walls, caused by the mass of the wall panels themselves and the stiffness of the cavity that separates them, also arises in both excitation problems.

1.2. Hypothesis

The authors have elucidated the fundamental relationship between sound radiations from airborne-sound-induced and force-excited vibrations for single-leaf structures through the use of a simple model [15]. Figure 1 provides a schematic explanation of the evaluation systems for airborne sound transmission and sound radiation from the force-excited vibration of solid boundaries, and a hypothesis on the relationship between the two problems. $\mathbf{M}_a$ and $\mathbf{M}_s$ are general evaluation indexes for each excitation problem. For example, the sound reduction indexes for random-incidence [2,3] and spherical incidence [16–18] are applicable to $\mathbf{M}_a$, and the radiation coefficient and radiation impedance are widely used for $\mathbf{M}_s$ [19–21]. In our previous study [15], the transmission coefficient for random incidence sound and the radiated sound power

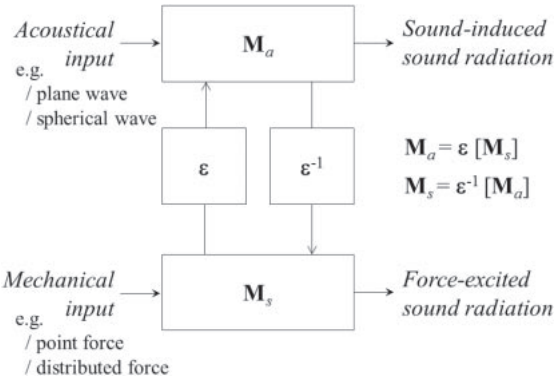

Fig. 1 Schematic diagram of evaluation systems showing the hypothesis regarding the relationship between sound radiations from airborne-sound-induced and force-excited vibrations of solid boundaries. The linear operator $\boldsymbol{\varepsilon}$ exists in a form independent of the parameters of boundaries [15].

under point-force excitation were introduced into $\mathbf{M}_a$ and $\mathbf{M}_s$, respectively. In the model, $\mathbf{M}_a$ and $\mathbf{M}_s$ are linked using a linear operator $\boldsymbol{\varepsilon}$ as follows:

$$\begin{cases} \mathbf{M}_a = \boldsymbol{\varepsilon}[\mathbf{M}_s] \\ \mathbf{M}_s = \boldsymbol{\varepsilon}^{-1}[\mathbf{M}_a] \end{cases}. \tag{1}$$

Note that $\boldsymbol{\varepsilon}$ must exist in a form independent of the parameters of walls, floors and any other solid boundaries. The transmission coefficient for random-incidence sound and the radiated sound power under the point-force excitation of a single-leaf infinite elastic plate have both been analyzed, and the existence of $\boldsymbol{\varepsilon}$ for single-leaf structures has been shown. $\boldsymbol{\varepsilon}$ is a function of only the specific impedance and the acoustic wavenumber of the medium, and is independent of all elastic plate parameters.

The purpose of the present work is to also reveal the existence of the linear operator $\boldsymbol{\varepsilon}$ in the case of double-leaf structures. In this paper, the sound radiation from a double-leaf infinite elastic plate driven by random-incidence sound in addition to that driven by point-force excitation are both analyzed. Exact solutions of the transmission coefficient for random-incidence sound, $\mathbf{M}_a$, and the radiated sound power under point-force excitation, $\mathbf{M}_s$, are also derived. Approximate solutions of $\mathbf{M}_a$ and $\mathbf{M}_s$ are also analyzed within the frequency range below the mass-air-mass resonance frequency. To verify the fundamental relationship between the two problems in a form independent of the parameters of the plates, we have to reveal that they are linked using a simple equation that can be physically interpreted. In our previous study regarding a single-leaf elastic plate, we focused on the approximation only applicable to low frequencies. In that case, the approximate solutions derived for both problems showed good agreement with the exact ones at low frequencies, and they also captured the overall slope of the exact ones. This tendency

has contributed to elucidating the relationship between the two problems regarding the single-leaf elastic plate. This can also be used as an analogy to explain a double-leaf elastic plate.

Then, a conversion function that relates the two problems is derived through the approximate solutions and compared with that derived for the single-leaf infinite elastic plate model developed in the previous study. Finally, numerical calculations are carried out to verify that the conversion function is also able to provide a relationship between the exact solutions.

As mentioned above, double-leaf walls, double-leaf ceilings, double-leaf floors and other double-leaf structures are widely used to reduce noise transmission arising from both airborne sound and structure-borne noise. If the linear operator $\boldsymbol{\varepsilon}$ for double-leaf structures can also be expressed in a form independent of all parameters of the plates, as has been shown for single-leaf structures, architectural acoustic calculations and predictions could be greatly simplified. For example, the airborne sound insulation performance of single-leaf and double-leaf structures for random-incidence sound could be estimated from measurement data of their radiated sound power under point-force excitation, and vice versa, without knowing any parameters of the structures themselves.

2. TRANSMISSION COEFFICIENT FOR RANDOM-INCIDENCE SOUND

2.1. Theoretical Considerations

Consider the double-leaf infinite elastic plate shown in Fig. 2 that is composed of two single plates lying on the planes $z = 0$ and $z = z_1$. Both plates are subjected to vibration under a plane wave incident at the angle Θ.

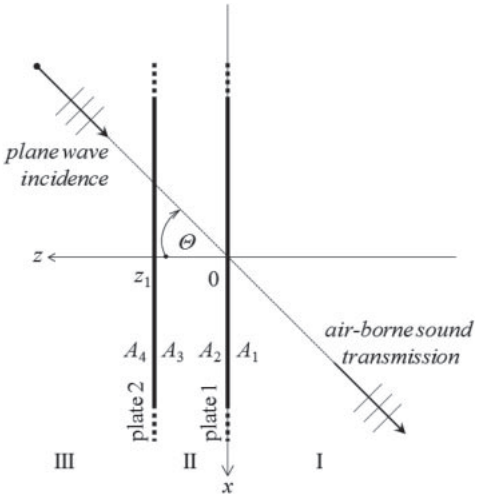

Fig. 2 Analytical model of a double-leaf infinite elastic plate using thin-plate theory. The plates vibrate and radiate sound driven by an incident oblique plane wave.

Suppose that the vibration of the plates is in accordance with classical thin-plate theory. The transmitted sound field is derived by simultaneously solving the governing equations of the sound field in addition to the motion of the plates. In this case, the transmission coefficient for the oblique-incidence sound $\tau(\Theta, \omega)$ is defined by the ratio of the incident sound power at the angle Θ to the transmitted sound power at the same angle. Several solutions to find the transmission coefficient in such a scenario have already been derived [22,23].

This paper refers to the procedures from Kiyama *et al.* [23] who theoretically investigated the acoustic characteristics of a double-leaf infinite membrane and derived the transmission coefficient for oblique-incidence sound. The exact solution of $\tau(\Theta, \omega)$ in the present model is obtained by replacing the unit response of the membrane, as presented in [23], with the unit response of the thin plate presented in this paper. This substitution yields

$$\tau(\Theta, \omega) = \left| \frac{\cos\Theta}{(\cos\Theta + A_1)(\cos\Theta + A_4)} \frac{2\rho_0 c_0 \omega}{\Psi(k_0 \sin\Theta)} \right|^2, \quad (2)$$

where

$$\Psi(k) = \frac{\Phi_1(k)\Phi_2(k)}{\dfrac{2\rho_0 c_0 \omega \cos\Theta}{\xi(\Theta)}} + \frac{2\rho_0 c_0 \omega \cos\Theta}{\xi(\Theta)}, \quad (3)$$

$$\Phi_1(k) = U_1(k) - i\rho_0 c_0 \omega \left(\frac{1}{\cos\Theta + A_1} + \frac{\zeta_3(\Theta)}{\xi(\Theta)} \right), \quad (4)$$

$$\Phi_2(k) = U_2(k) - i\rho_0 c_0 \omega \left(\frac{1}{\cos\Theta + A_4} + \frac{\zeta_2(\Theta)}{\xi(\Theta)} \right), \quad (5)$$

$$\xi(\Theta) = (\cos\Theta + A_2)(\cos\Theta + A_3)e^{-i\varphi(\Theta)} - (\cos\Theta - A_2)(\cos\Theta - A_3)e^{i\varphi(\Theta)}, \quad (6)$$

$$\zeta_2(\Theta) = (\cos\Theta + A_2)e^{-i\varphi(\Theta)} + (\cos\Theta - A_2)e^{i\varphi(\Theta)}, \quad (7)$$

$$\zeta_3(\Theta) = (\cos\Theta + A_3)e^{-i\varphi(\Theta)} + (\cos\Theta - A_3)e^{i\varphi(\Theta)}, \quad (8)$$

$$\varphi(\Theta) = k_0 z_1 \cos\Theta, \quad (9)$$

$$U_j(k) = D_j k^4 - \rho_{pj} h_j \omega^2, \quad j = 1, 2. \quad (10)$$

Above, k_0 is the acoustic wavenumber in air, ω the angular frequency, c_0 the speed of sound in air, ρ_0 the air density, and the flexural rigidity of the plate number j is represented by $D_j = E_j(1 - i\eta_j)h_j^3/12(1 - \nu_j^2)$. E_j represents Young's modulus, h_j the thickness, η_j the loss factor, ν_j Poisson's ratio and ρ_{pj} the density of each plate. The acoustic admittances A_1–A_4 of both sides of the plates are also considered in this analysis. In the case of vibrating surfaces assumed to be locally reacting with the velocity v under the sound pressure p, the particle velocity of the surface would appear to be $v + p/Z$, in which Z denotes the acoustic impedance of the surface; thus, the acoustic admittance A is defined as $A = \rho_0 c_0 / Z$ [24]. It is known

that the acoustic admittance in the cavity affects the mass-air-mass resonance.

The transmission coefficient for random-incidence sound is defined as the ratio of the transmitted sound power to the incident sound power from all directions. The transmission coefficient for random-incidence sound is obtained by averaging the coefficients for oblique incidence over a hemisphere. This approach, which is based on a completely diffuse sound field, does not fully reflect the actual conditions in rooms, and so various methods of truncating the incidence angle up to a certain limit have been proposed [2,25]. In general, this is calculated by integrating over the range of $\Theta = 0$–78° because of the good agreement with experimental results. The transmission coefficient for random-incidence sound, $\tau(\omega)$, is therefore derived from the following integration:

$$\tau(\omega) = \frac{\displaystyle\int_0^{78} \tau(\Theta,\omega)\cos\Theta\sin\Theta\, d\Theta}{\displaystyle\int_0^{78} \cos\Theta\sin\Theta\, d\Theta}. \tag{11}$$

2.2. Approximate Solution

The integral in Eq. (11) is evaluated analytically within a low-frequency limit. The acoustic admittances A_1–A_4 are assumed to be zero and the following approximations are introduced into Eq. (2):

$$\omega^2 \ll \omega_c^2 = \frac{c_0^2 m_j}{\mathrm{Re}(D_j)}, \quad j = 1, 2, \tag{12}$$

where ω_c is the critical frequency, which is well known as the coincidence effect, and $m_j = \rho_{pj} h_j$ is the surface density of each plate. From these approximations, $\tau(\Theta,\omega)$ becomes

$$\tau(\Theta,\omega) \cong \left| \frac{1}{\cos\Theta} \frac{2\rho_0 c_0 \omega}{\Psi(\omega)} \right|^2, \tag{13}$$

where

$$\Psi(\omega) = \frac{\Phi_1(\omega)\Phi_2(\omega)}{i\dfrac{\rho_0 c_0^2}{z_1\cos^2\Theta}} + i\frac{\rho_0 c_0^2}{z_1\cos^2\Theta}, \tag{14}$$

$$\Phi_j(\omega) = \frac{\rho_0 c_0 \omega}{\cos\Theta}\left(i - \frac{1}{ik_0 z_1\cos\Theta}\right) - m_j\omega^2, \quad j = 1, 2. \tag{15}$$

The small-angle approximation has been included at the low-frequency limit. Here, we focus on the mass-air-mass resonance frequency of the double-leaf plate:

$$\omega_r^2(\Theta) = \frac{m_1 + m_2}{m_1 m_2}\frac{\rho_0 c_0^2}{z_1\cos^2\Theta}. \tag{16}$$

$\omega_r(\Theta)$ is the mass-air-mass resonance frequency under the condition of oblique plane-wave incidence, which depends on the angle of incidence [26]. Using $\omega_r(\Theta)$, $\tau(\Theta,\omega)$ can be expressed as

$$\tau(\Theta,\omega) \cong \left| \frac{-i}{\omega\cos\Theta} \frac{2\rho_0^2 c_0}{\dfrac{\rho_0 c_0^2(m_1+m_2)}{c_0^2}\dfrac{\omega^2}{\omega_r^2(\Theta)} - (m_1+m_2)\rho_0} \right|^2. \tag{17}$$

In Eq. (17), considering the further approximation $\omega^2 \ll {\omega_r}^2(\theta)$, $\tau(\Theta,\omega)$ becomes

$$\tau(\Theta,\omega) \cong \left[\frac{2\rho_0 c_0}{(m_1+m_2)\omega\cos\Theta}\right]^2. \tag{18}$$

The approximate solution of the transmission coefficient for random-incidence sound, $\hat{\tau}(\omega)$, is then derived by substituting Eq. (18) into Eq. (11):

$$\hat{\tau}(\omega) = 3.28\left[\frac{2\rho_0 c_0}{(m_1+m_2)\omega}\right]^2. \tag{19}$$

Numerical examples of Eqs. (11) and (19) are shown in Fig. 3. This figure also shows a comparison of the approximate solution (solid line) and the exact solution (broken line) in the case of $\rho_{p1} = \rho_{p2} = 1{,}000\,\mathrm{kg/m^3}$, $h_1 = h_2 = 20\,\mathrm{mm}$, $E_1 = E_2 = 1.8 \times 10^9\,\mathrm{N/m^2}$, $\eta_1 = \eta_2 = 0.03$, $\nu_1 = \nu_2 = 0.30$, $z_1 = 0.05\,\mathrm{m}$ and $A_1 = A_2 = A_3 = A_4 = 0.013$. The approximate solution is not in very good agreement with the exact one, but it can describe the overall slope of the exact one.

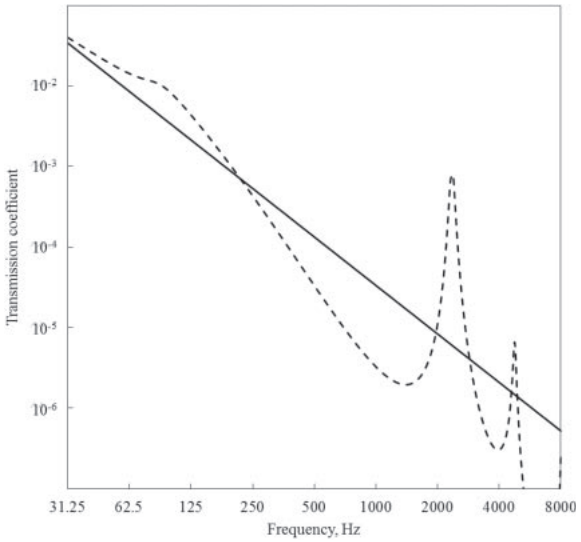

Fig. 3 Numerical examples of the transmission coefficient for random-incidence sound. Comparison of the approximate solution (solid line) and the exact solution (broken line) in the case of $\rho_{p1} = \rho_{p2} = 1{,}000\,\mathrm{kg/m^3}$, $h_1 = h_2 = 20\,\mathrm{mm}$, $E_1 = E_2 = 1.8 \times 10^9\,\mathrm{N/m^2}$, $\eta_1 = \eta_2 = 0.03$, $\nu_1 = \nu_2 = 0.30$, $z_1 = 0.05\,\mathrm{m}$ and $A_1 = A_2 = A_3 = A_4 = 0.013$.

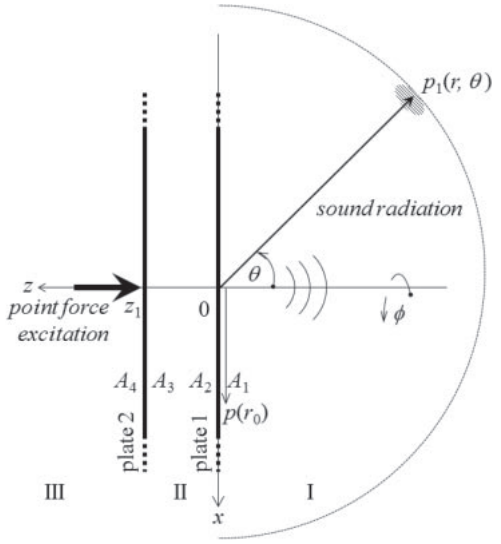

Fig. 4 Analytical model of a double-leaf infinite elastic plate using thin-plate theory. The plates vibrate and radiate sound driven by point-force excitation.

3. RADIATED SOUND POWER UNDER POINT-FORCE EXCITATION

3.1. Theoretical Considerations

Consider the double-leaf infinite elastic plate composed of Plates 1 and 2 in Fig. 4. Plate 2, lying in the plane $z = z_1$, vibrates as a result of being driven by the point force $F(\omega)$. Suppose that the vibration of the plates is in accordance with classical thin-plate theory. The radiated sound power from Plate 1 is derived by simultaneously solving the governing equations of the sound field and those for the motion of the plates. This problem was solved previously under the assumption that the acoustic admittance of the plates is zero, i.e., no absorption [27]. Exactly as in Sect. 2 for random-incidence airborne sound excitation, the acoustic admittances A_1–A_4 of both sides of the plates are also taken into account in this theory.

The sound pressures $p_1(\boldsymbol{r})$, $p_2(\boldsymbol{r})$ and $p_3(\boldsymbol{r})$ at a certain point $\boldsymbol{r}$ in Regions I, II and III (i.e. Fig. 4), respectively, are expressed by the following integrals:

$$p_1(\boldsymbol{r}) = \iint_S \frac{\partial p_1(\boldsymbol{r})}{\partial n_0} G(\boldsymbol{r}|\boldsymbol{r}_0) dS_0, \tag{20}$$

$$p_2(\boldsymbol{r}) = \iint_S \frac{\partial p_2(\boldsymbol{r})}{\partial n_0} G_p(\boldsymbol{r}|\boldsymbol{r}_0) dS_0, \tag{21}$$

$$p_3(\boldsymbol{r}) = \iint_S \frac{\partial p_3(\boldsymbol{r})}{\partial n_0} G(\boldsymbol{r}|\boldsymbol{r}_0) dS_0. \tag{22}$$

The double integral denotes the integral over all regions of the boundary and n_0 is the outward normal of each region. In Regions I and III, $\mathrm{G}(\boldsymbol{r}|\boldsymbol{r}_0)$ denotes the Green's function satisfying the Neumann condition for a single boundary with infinite extent and is expressed in the cylindrical coordinate system, where $\boldsymbol{r} = (\boldsymbol{\rho}, z) = (r, \phi, z)$ and $\boldsymbol{r}_0 = (\boldsymbol{\rho}_0, z) = (r_0, \phi_0, z_0)$. Thus, $\mathrm{G}(\boldsymbol{r}|\boldsymbol{r}_0)$ can be expressed as

$$G(\boldsymbol{r}|\boldsymbol{r}_0) = \int_0^\infty \frac{J_0(k|\boldsymbol{\rho} - \boldsymbol{\rho}_0|)}{4\pi\gamma(k)} \exp(-\gamma(k)|z \pm z_0|) k dk, \tag{23}$$

where

$$\gamma(k) = \sqrt{k^2 - k_0^2}. \tag{24}$$

In Region II, the Green's function should satisfy the Neumann condition for parallel infinite boundaries such that $\mathrm{G}_p(\boldsymbol{r}|\boldsymbol{r}_0)$ is used instead of $\mathrm{G}(\boldsymbol{r}|\boldsymbol{r}_0)$, which is expressed as [28]

$$G_p(\boldsymbol{r}|\boldsymbol{r}_0) = \int_0^\infty \frac{J_0(k|\boldsymbol{\rho} - \boldsymbol{\rho}_0|)}{2\pi\gamma(k)} \times \frac{\cosh(\gamma(k)|z_1 - z|)\cosh(\gamma(k)z_0)}{\sinh(\gamma(k)z_1)} k dk. \tag{25}$$

The boundary conditions of the plate surfaces are

$$\left.\frac{\partial p_1(\boldsymbol{r})}{\partial n_0}\right|_{z=0} = \left.\frac{\partial p_1(\boldsymbol{r})}{\partial z}\right|_{z=0} = \rho_0\omega^2 w_1(r) + ik_0 A_1 p_1(r, 0), \tag{26}$$

$$\left.\frac{\partial p_2(\boldsymbol{r})}{\partial n_0}\right|_{z=0} = -\left.\frac{\partial p_2(\boldsymbol{r})}{\partial z}\right|_{z=0} = -\rho_0\omega^2 w_1(r) + ik_0 A_2 p_1(r, 0), \tag{27}$$

$$\left.\frac{\partial p_2(\boldsymbol{r})}{\partial n_0}\right|_{z=z_1} = \left.\frac{\partial p_2(\boldsymbol{r})}{\partial z}\right|_{z=z_1} = \rho_0\omega^2 w_2(r) + ik_0 A_3 p_2(r, z_1), \tag{28}$$

$$\left.\frac{\partial p_3(\boldsymbol{r})}{\partial n_0}\right|_{z=z_1} = -\left.\frac{\partial p_3(\boldsymbol{r})}{\partial z}\right|_{z=z_1} = -\rho_0\omega^2 w_2(r, z_1) + ik_0 A_4 p_3(r, z_1). \tag{29}$$

The displacement of Plate 1, $w_1(r)$, and that of Plate 2, $w_2(r)$, are expressed by the following equations of motion:

$$(D_1\nabla^4 - \rho_{p1}h_1\omega^2) w_1(r) = p_1(r, 0) - p_2(r, 0), \tag{30}$$

$$(D_2\nabla^4 - \rho_{p2}h_2\omega^2) w_2(r) = p_2(r, z_1) - p_3(r, z_1) - \frac{F(\omega)\delta(r)}{2\pi r}, \tag{31}$$

where $\delta(r)$ is the Dirac delta function. Assuming the problem to be axisymmetric and using of the Hankel transform in cylindrical coordinates, the angular spectrum $W_1(k)$ with respect to $w_1(r_0)$ can be obtained in the same manner as in the previous study [27] and is expressed as

$$W_1(k) = -\frac{1}{2\pi} \frac{F(\omega)}{\dfrac{R_1(k)R_2(k)}{Q_2(k)} - Q_3(k)}, \tag{32}$$

where

$$R_1(k) = U_1(k) - \frac{\rho_0\omega^2}{\gamma(k) - ik_0A_1} - Q_1(k), \tag{33}$$

$$R_2(k) = U_2(k) - \frac{\rho_0\omega^2}{\gamma(k) - ik_0A_4}\frac{1+\exp(-\gamma(k)2z_1)}{2} - Q_4(k), \tag{34}$$

$$Q_1(k) = \frac{\frac{\rho_0\omega^2}{\gamma(k)}\cosh(\gamma(k)z_1)}{1 - \frac{ik_0A_2}{\gamma(k)}\cosh(\gamma(k)z_1) - \frac{ik_0A_3}{\gamma(k)}\frac{1}{\sinh(\gamma(k)z_1)}}, \tag{35}$$

$$Q_2(k) = \frac{\frac{\rho_0\omega^2}{\gamma(k)}\frac{1}{\sinh(\gamma(k)z_1)}}{1 - \frac{ik_0A_2}{\gamma(k)}\cosh(\gamma(k)z_1) - \frac{ik_0A_3}{\gamma(k)}\frac{1}{\sinh(\gamma(k)z_1)}}, \tag{36}$$

$$Q_3(k) = \frac{\frac{\rho_0\omega^2}{\gamma(k)}\frac{1}{\sinh(\gamma(k)z_1)}}{1 - \frac{ik_0A_2}{\gamma(k)}\frac{1}{\sinh(\gamma(k)z_1)} - \frac{ik_0A_3}{\gamma(k)}\cosh(\gamma(k)z_1)}, \tag{37}$$

$$Q_4(k) = \frac{\frac{\rho_0\omega^2}{\gamma(k)}\cosh(\gamma(k)z_1)}{1 - \frac{ik_0A_2}{\gamma(k)}\frac{1}{\sinh(\gamma(k)z_1)} - \frac{ik_0A_3}{\gamma(k)}\cosh(\gamma(k)z_1)}, \tag{38}$$

$W_1(k)$ and $w_1(r_0)$ are related to the Hankel transform defined by the following equations:

$$\begin{cases} W_1(k) = \int_0^\infty w_1(r_0)J_0(kr_0)r_0dr_0 \\ w_1(r_0) = \int_0^\infty W_1(k)J_0(kr_0)kdk \end{cases}. \tag{39}$$

The sound pressure on Plate 1, $p_1(r,0)$, is expressed using $W_1(k)$ as

$$p_1(r,0) = \rho_0\omega^2\int_0^\infty \frac{W_1(k)}{i\gamma(k) + k_0A_1}J_0(kr)kdk. \tag{40}$$

The exact solution of the radiated sound power under point-force excitation, $\Pi(\omega)$, is obtained by integrating the surface intensity of Plate 1 over the entire infinite surface. Thus,

$$\Pi(\omega) = \iint_S \mathrm{Re}\left[\frac{1}{2}p_1(r,0)\bar{v}_1(r)\right]dS_0, \tag{41}$$

where

$$v_1(r) = -i\omega w_1(r) = -i\omega\int_0^\infty W_1(k)J_0(kr)kdk \tag{42}$$

is the velocity of Plate 1 and $\bar{v}_1(r)$ is its complex conjugate. Substituting Eqs. (40) and (42) into Eq. (41), $\Pi(\omega)$ can now be expressed by the following integral:

$$\begin{aligned}\Pi(\omega) &= \pi\rho_0\omega^3\,\mathrm{Re}\left[\int_0^\infty dk\int_0^\infty dk'\,\frac{W_1(k)\bar{W}_1(k')}{i\gamma(k)+k_0A_1}kk' \times\int_0^\infty J_0(kr)J_0(k'r)rdr\right] \\ &= \pi\rho_0\omega^3\,\mathrm{Re}\left[\int_0^\infty kdk\int_0^\infty \frac{W_1(k)\bar{W}_1(k')}{i\gamma(k)+k_0A_1}\delta(k-k')dk'\right] \\ &= \pi\rho_0\omega^3\int_0^{k_0}\frac{|W_1(k)|^2}{\sqrt{k_0^2-k^2}+k_0A_1}kdk. \end{aligned}\tag{43}$$

Here, the following integral representation for the Dirac delta function has been used [29]:

$$k'\int_0^\infty J_0(kr)J_0(k'r)rdr = \delta(k-k'). \tag{44}$$

The radiated sound power $\Pi(\omega)$ is normalized by the point force $F(\omega)$.

3.2. Approximate Solution

The radiated sound power under point-force excitation can also be obtained by integrating the radial intensity in the far field [27]. In Fig. 4, θ denotes the polar angle between the direction of the receiving point and the negative direction of the z-axis. Using Rayleigh's integral [12], the approximate solution of the radiated sound pressure $p_1(r,\theta)$ is obtained from Eq. (20) and expressed in closed form as

$$\begin{aligned} p_1(r,\theta) &\cong \rho_0\omega^2W_1(k_0\sin\theta)\frac{\exp(ik_0r)}{r} \\ &= -\frac{2\rho_0\omega^2}{K(\omega)}F(\omega)\frac{\exp(ik_0r)}{4\pi r}, \end{aligned}\tag{45}$$

where

$$K(\omega) = \frac{R_1(\omega)R_2(\omega)}{\frac{\rho_0c_0\omega}{\cos\theta}\frac{1}{\sin\varphi(\theta)}} + \frac{\rho_0c_0\omega}{\cos\theta}\frac{1}{\sin\varphi(\theta)}, \tag{46}$$

$$R_1(\omega) = \frac{\rho_0c_0\omega}{\cos\theta}(1 + i\cot\varphi(\theta)) + iU_1(\omega), \tag{47}$$

$$R_2(\omega) = \frac{\rho_0c_0\omega}{\cos\theta}\left[\frac{1+\exp(i\varphi(\theta))}{2} + i\cot\varphi(\theta)\right] + iU_2(\omega), \tag{48}$$

$$\varphi(\theta) = k_0z_1\cos\theta. \tag{49}$$

In the above derivation, the acoustic admittances A_1–A_4 are assumed to be zero. Integrating the radial intensity $|p_1(r,\theta)|/2\rho_0c_0$ over a hemisphere of radius r yields the approximate solution of the radiated sound power under point-force excitation, $\hat{\Pi}(\omega)$; thus,

$$\hat{\Pi}(\omega) \cong \frac{r^2}{2\rho_0c_0}\int_0^{2\pi}d\varphi\int_0^{\pi/2}|p_1(r,\theta)|^2\sin\theta\,d\theta. \tag{50}$$

As in the case of random-incidence sound, further approx-

imations are introduced. Defining the mass-air-mass resonance frequency ω_r in a form independent of the angle θ,

$$\omega_r^2 = \frac{m_1 + m_2}{m_1 m_2}\frac{\rho_0 c_0^2}{z_1}. \tag{51}$$

Equation (45) can now be rewritten as

$$p_1(r,\theta) \cong \frac{\dfrac{2\rho_0}{m_1+m_2}\dfrac{\omega_r^2}{\omega^2}}{\cos^2\theta - \dfrac{\omega_r^2}{\omega^2}} F(\omega)\frac{\exp(ik_0 r)}{4\pi r}. \tag{52}$$

Equation (52) also includes the small-angle approximation at the low-frequency limit, where $\omega^2/{\omega_c}^2$ is negligible. The integral in Eq. (50) is evaluated analytically within the low-frequency limit so that the approximate solution of the radiated sound power $\hat{\Pi}(\omega)$ can be obtained in closed form as

$$\hat{\Pi}(\omega) = \frac{1}{4\pi\rho_0 c_0}\left(\frac{\rho_0}{m_1+m_2}\right)^2 \times \left[\frac{1}{2}\frac{\omega_r^2}{\omega_r^2-\omega^2} + \frac{1}{2}\frac{\omega_r}{\omega}\tanh^{-1}\frac{\omega}{\omega_r}\right], \tag{53}$$

where $\hat{\Pi}(\omega)$ is normalized by $F(\omega)$. The two summation terms in the square brackets represent the acoustical coupling between the two plates and are nearly equal to one under the condition of $\omega \ll \omega_r$; thus, Eq. (53) can be further simplified to yield

$$\hat{\Pi}(\omega) \cong \frac{1}{4\pi\rho_0 c_0}\left(\frac{\rho_0}{m_1+m_2}\right)^2. \tag{54}$$

Numerical examples of Eqs. (43) and (54) are shown in Fig. 5. This figure also shows a comparison of the approximate solution (solid line) and the exact solution (broken line) in the case of $\rho_{p1} = \rho_{p2} = 1{,}000\,\mathrm{kg/m^3}$, $h_1 = h_2 = 20\,\mathrm{mm}$, $E_1 = E_2 = 1.8 \times 10^9\,\mathrm{N/m^2}$, $\eta_1 = \eta_2 = 0.03$, $\nu_1 = \nu_2 = 0.30$, $z_1 = 0.05\,\mathrm{m}$ and $A_1 = A_2 = A_3 = A_4 = 0.013$. The approximate solution is not in very good agreement with the exact one, but it can describe the overall slope of the exact one.

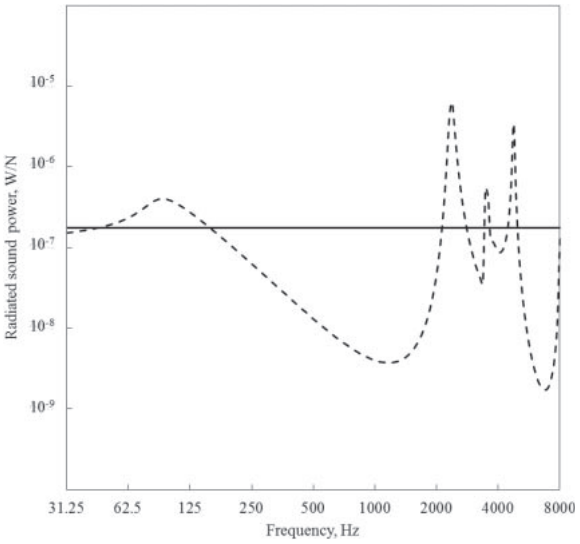

Fig. 5 Examples of calculated radiated sound power driven by point force. Comparison of the approximate solution (solid line) and the exact solution (broken line) in the case of $\rho_{p1} = \rho_{p2} = 1{,}000\,\mathrm{kg/m^3}$, $h_1 = h_2 = 20\,\mathrm{mm}$, $E_1 = E_2 = 1.8 \times 10^9\,\mathrm{N/m^2}$, $\eta_1 = \eta_2 = 0.03$, $\nu_1 = \nu_2 = 0.30$, $z_1 = 0.05\,\mathrm{m}$ and $A_1 = A_2 = A_3 = A_4 = 0.013$.

4. RELATIONSHIP BETWEEN THE TWO EXCITATION PROBLEMS

4.1. Derivation of Conversion Function

From the approximate solutions of the transmission coefficient for random-incidence sound, $\hat{\tau}(\omega)$, in Eq. (19) and the radiated sound power under point-force excitation, $\hat{\Pi}(\omega)$, in Eq. (54), the following relation can be derived:

$$\hat{\tau}(\omega) = \varepsilon(\omega)\hat{\Pi}(\omega), \tag{55}$$

where the conversion function $\varepsilon(\omega)$ is defined as

$$\varepsilon(\omega) \cong \frac{52\pi\rho_0 c_0}{k_0^2}. \tag{56}$$

$\varepsilon(\omega)$ is a function of the specific impedance $\rho_0 c_0$ and the acoustic wavenumber k_0 of the medium on either side of the double-leaf plate, and does not include any parameters of the plates themselves or the cavity between them. This implies that the linear operator $\boldsymbol{\varepsilon}$, defined in Eq. (1), exists in a form independent of all parameters of the plates within the low-frequency limit under the mass-air-mass resonance frequency. Moreover, the conversion function $\varepsilon(\omega)$ derived for a double-leaf infinite elastic plate model is in agreement with the same function derived for a single-leaf infinite elastic plate model [15]. The physical meaning of $\varepsilon(\omega)$ has been considered in detail in previous studies [15,29]. The characteristics of $\varepsilon(\omega)$ as a function of frequency are shown in Fig. 6 since the frequency characteristics in the audible frequency range are meaningful in building acoustics.

4.2. Application of the Conversion Function to the Exact Solutions

The conversion function $\varepsilon(\omega)$ derived through the discussion thus far has been obtained from the relationship between the approximate solutions; therefore, it is not clear whether $\varepsilon(\omega)$ can provide any meaningful relationship between the exact solutions. In this section, the possibility of applying $\varepsilon(\omega)$ to the exact solutions, namely,

$$\tau(\omega) \cong \varepsilon(\omega)\Pi(\omega), \tag{57}$$

is verified by two sample construction calculations. Note that the exact solutions $\tau(\omega)$ and $\Pi(\omega)$ are given by Eqs. (11) and (43), respectively.

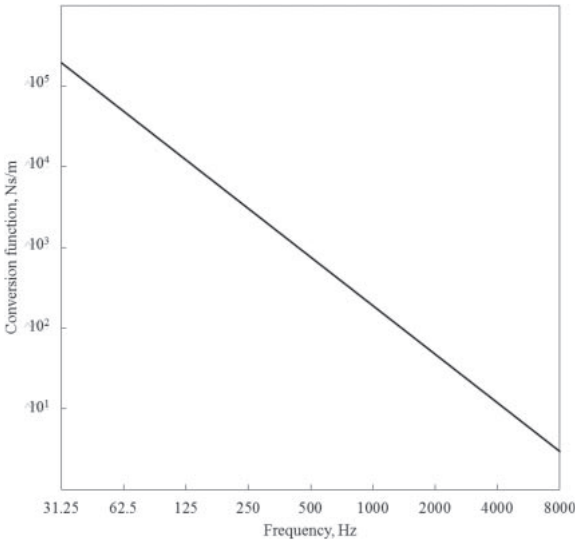

Fig. 6 Frequency characteristics of the conversion function $\varepsilon(\omega)$ given in Eq. (56), which agrees with the conversion function derived from a single-leaf infinite elastic plate model.

Table 1 Physical parameters of double-leaf elastic plates used in the calculations.

Parameters*	(a)**		(b)***	
	Plate 1	Plate 2	Plate 1	Plate 2
Young's modulus, E_j, N/m^2	1.8×10^9	2.6×10^{10}	1.8×10^9	1.8×10^9
Thickness, h_j, m	0.03	0.25	0.03	0.03
Loss factor, η_j	0.03	0.005	0.03	0.03
Poisson's ratio, ν_j	0.30	0.20	0.30	0.30
Density, ρ_{pj}, kg/m^3	1,300	2,400	650	650
Cavity depth, z_1, m	0.03		0.05	

*$j = 1, 2$ denote Plates 1 and 2, respectively
**Reinforced concrete panel + gypsum board
***Gypsum board + gypsum board

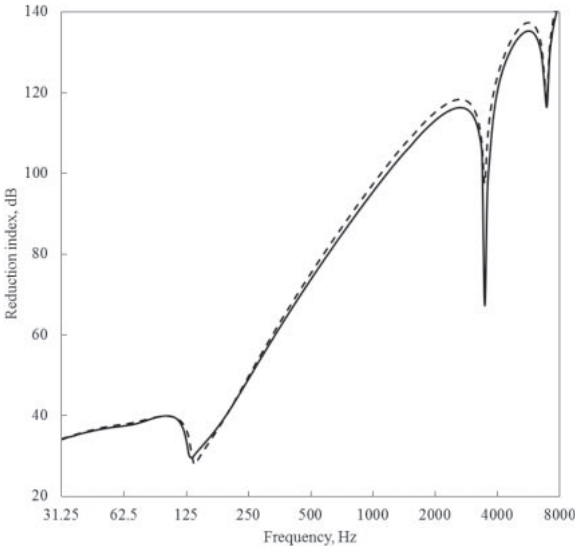

(a)

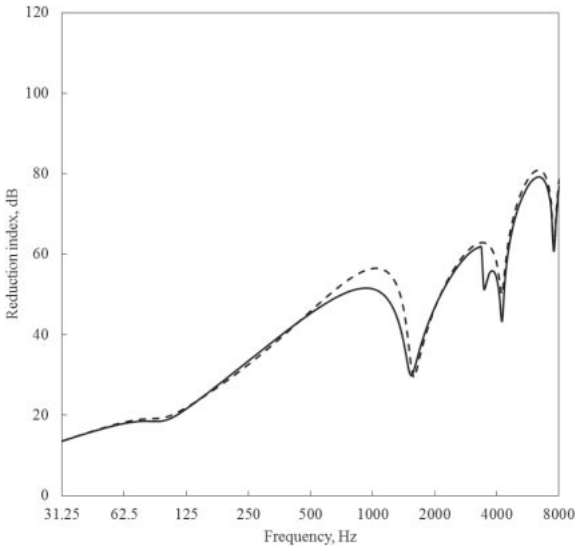

(b)

Fig. 7 Sample of double-leaf wall construction calculations based on the conversion function between exact solutions given by Eq. (57). The calculated results represent the two considered construction cases of (a) reinforced concrete panel + gypsum board and (b) gypsum board + gypsum board. The dashed line represents the inverse of $\tau(\omega)$ in decibels (reduction index) and the solid line represents the inverse of $\varepsilon(\omega)\Pi(\omega)$ in decibels. These results assume $A_1 = A_2 = A_3 = A_4 = 0.013$.

Table 1 provides two typical wall construction cases that have been assumed as examples of elastic plate calculations. The two sample double-leaf wall constructions consist of (a) reinforced concrete panel + gypsum board and (b) gypsum board + gypsum board. In the calculations, the reciprocal of both sides in Eq. (57) is considered to obtain the sound reduction index for airborne sound insulation, namely, $10\log_{10}\tau^{-1}(\omega)$ and $10\log_{10}[\varepsilon^{-1}(\omega)\Pi^{-1}(\omega)]$ are compared.

Figure 7 shows the results calculated under the conditions of $A_1 = A_2 = A_3 = A_4 = 0.013$ to estimate a common degree of cavity damping. This assumption corresponds to an equivalent sound absorption coefficient of 5%. The acoustic admittance was originally defined as the ratio of the specific impedance of air, $\rho_0 c_0$, to the surface acoustic impedance of the plate. Therefore, the acoustic admittance has normally been given by a complex number that depends on the frequency. However, in this paper, we assumed that it is a constant real number independent of the frequency to clarify the effect of the acoustic admittance itself. The typical behavior of the reduction index is characterized by significant dips around the mass-air-mass resonance (100–200 Hz) and the higher-order resonance (above 3 kHz). The dip at the critical frequency (around 1.8 kHz) caused by the coincidence

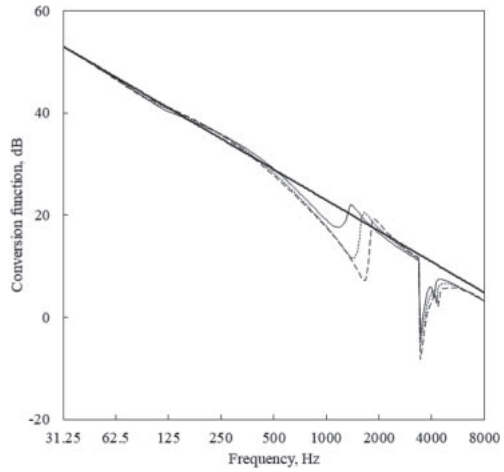

(a) Effect of the density of the plates on the conversion function: $\rho_{p1} = \rho_{p2} =$ 500 (thin line), 700 (dotted line) and 900 (broken line) kg/m^3, and $\varepsilon(\omega)$ in Eq. (56) (thick line). Other parameters are the same as in Table 1 (b).

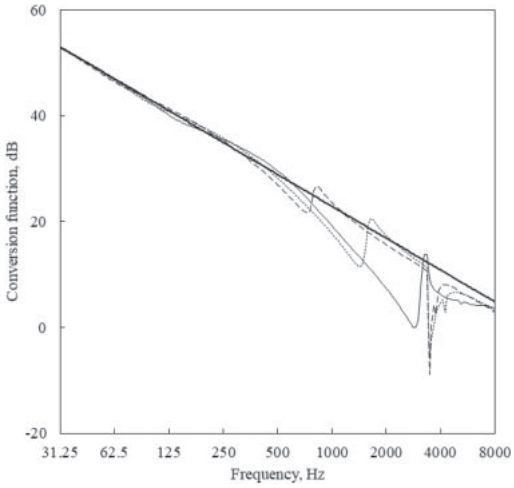

(b) Effect of the thickness of the plates on the conversion function: $h_1 = h_2 =$ 0.0125 (thin line), 0.025 (dotted line) and 0.05 (broken line) kg/m^3, and $\varepsilon(\omega)$ in Eq. (56) (thick line). Other parameters are the same as in Table 1(b).

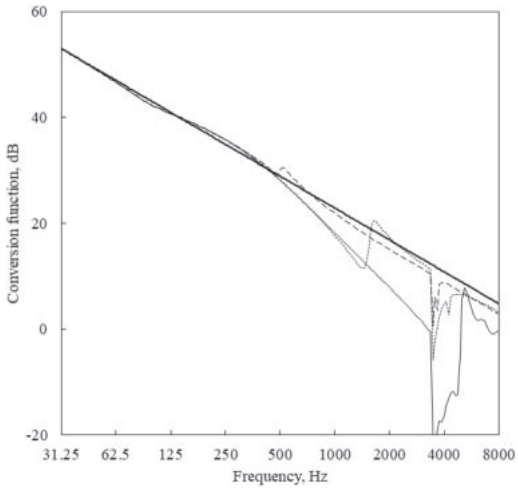

(c) Effect of Young's modulus of the plates on the conversion function: $E_1 =$ $E_2 = 1.8\times10^8$ (thin line), 1.8×10^9 (dotted line) and 1.8×10^{10} (broken line) N/m^2, and $\varepsilon(\omega)$ in Eq. (56) (thick line). Other parameters are the same as in Table 1(b).

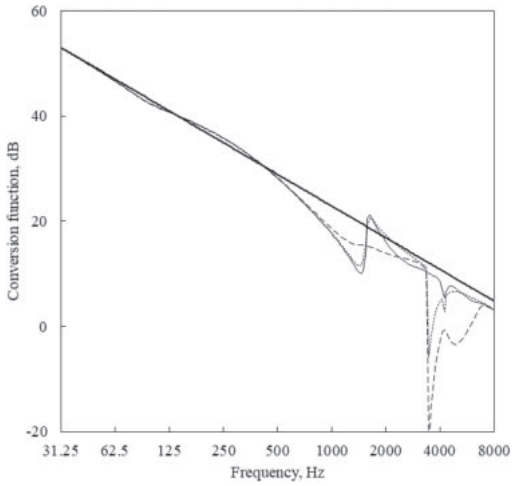

(d) Effect of the loss factor of the plates on the conversion function: $\eta_1 =$ $\eta_2 = 0.005$ (thin line), 0.05 (dotted line) and 0.5 (broken line), and $\varepsilon(\omega)$ in Eq. (56) (thick line). Other parameters are the same as in Table 1(b).

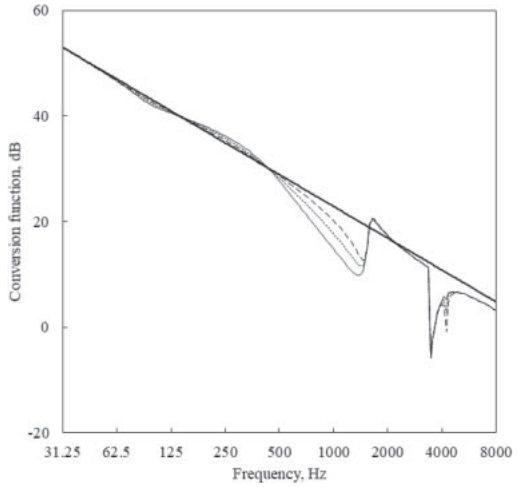

(e) Effect of the acoustic admittance of the plates on the conversion function: $A_2 = A_3 = 0.007$ (thin line), 0.013 (dotted line) and 0.026 (broken line), and $\varepsilon(\omega)$ in Eq. (56) (thick line). Other parameters are the same as in Table 1(b).

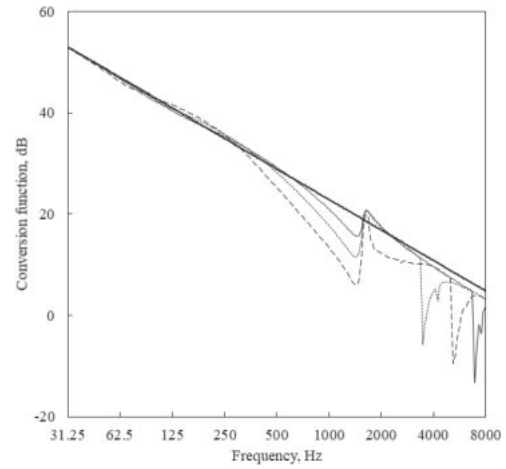

(f) Effect of the cavity depth of the plates on the conversion function: $z_1 =$ 0.025 (thin line), 0.05 (dotted line) and 0.1 (broken line) m, and $\varepsilon(\omega)$ in Eq. (56) (thick line). Other parameters are the same as in Table 1(b).

Fig. 8 Results of parametric studies.

effect of the gypsum boards in construction case (b) (see Fig. 7(b)) does not appear in construction case (a) (see Fig. 7(a)). The results for the reduction index calculated via the transmission coefficient and the converted radiated sound power under point-force excitation are in fairly good agreement at all frequencies in Fig. 7(a). On the other hand, large differences arise around mid-frequencies in Fig. 7(b), and this may be caused by a difference in cavity behavior. Therefore, parametric studies based on case (b) are carried out in the following section.

4.3. Parametric Studies

Parametric studies based on the case of (b) gypsum board + gypsum board with the parameters in Table 1 are carried out. The parameters of the plates considered are the density $\rho_{p1} = \rho_{p2} = 500, 700, 900\,\mathrm{kg/m^3}$, the thickness $h_1 = h_2 = 0.0125, 0.025, 0.05\,\mathrm{m}$, Young's modulus $E_1 = E_2 = 1.8 \times 10^8, 1.8 \times 10^9, 1.8 \times 10^{10}\,\mathrm{N/m^2}$, the loss factor $\eta_1 = \eta_2 = 0.005, 0.05, 0.5$, the acoustic admittance $A_2 = A_3 = 0.007, 0.013, 0.026$ of the plates and the cavity depth $z_1 = 0.025, 0.05, 0.1\,\mathrm{m}$. Results are shown in Figs. 8(a)–8(f). In the calculations, $\varepsilon(\omega)$ in Eq. (56) and $\tau^{-}(\omega)/\Pi(\omega)$ are compared in decibels. The effects of the density (a), thickness (b), Young's modulus (c), loss factor (d) and acoustic admittance (e) are similar tendencies: the overall slopes of $\tau^{-}(\omega)/\Pi(\omega)$ are in very good agreement with that of $\varepsilon(\omega)$ and the values almost coincide below the mid-frequency (500 Hz). The effect of the cavity depth is slightly different from the others: the discrepancy between $\tau^{-}(\omega)/\Pi(\omega)$ and $\varepsilon(\omega)$ starts from lower frequencies with increasing cavity depth, since the acoustic coupling between the plates decreases with increasing cavity depth.

5. CONCLUSIONS

In this paper, a theory for relating random-incidence sound-induced and point-force-excited sound radiations from solid structures was expanded from the previously established single-leaf elastic plate model to a double-leaf infinite elastic plate model. The conversion function established in this paper, relating the two sources of excitation for a double-leaf infinite elastic plate model, agrees with the previously established conversion function derived for a single-leaf infinite elastic plate model.

The sound radiation from a double-leaf infinite elastic plate driven by random-incidence sound and that driven by point-force excitation were both analyzed, and the exact solutions of the transmission coefficients for each source of excitation were derived. Approximate solutions of these problems were also derived from the exact solutions within the low-frequency limit below the mass-air-mass resonance frequency. The conversion function that relates the two problems was obtained in a simple closed form through the approximate solutions. This function includes only the specific impedance and the acoustic wavenumber of the medium surrounding the plates and does not include any parameters of the plates or the cavity between them. Sample calculations verified that the conversion function was able to linearly relate the exact solutions at low and mid frequencies including above the mass-air-mass resonance frequency.

ACKNOWLEDGMENTS

The authors would like to thank Mr. Kosuke Nishibara for his collaborative assistance in the present work and Christopher Buckley for his thorough review of the paper's English.

REFERENCES

[1] L. Cremer, M. Heckl and B. A. T. Petersson, *Structure-Borne Sound: Structural Vibrations and Sound Radiation at Audio Frequencies*, 3rd ed. (Springer, Berlin, 2005), Chap. 1.
[2] L. L. Beranek and I. L. Vér, *Noise and Vibration Control Engineering: Principles and Applications* (John Wiley & Sons, New York, 1992), Chap. 11.
[3] Z. Maekawa, J. H. Rindel and P. Lord, *Environmental and Architectural Acoustics*, 2nd ed. (CRC Press, Boca Raton, 2011), Chap. 5.
[4] S. Nakanishi, M. Yairi and A. Minemura, "Estimation method for parameters of construction on predicting transmission loss of double leaf dry partition," *Appl. Acoust.*, **72**, 364–371 (2011).
[5] J. L. Davy, "The improvement of a simple theoretical model for the prediction of the sound insulation of double leaf walls," *J. Acoust. Soc. Am.*, **127**, 841–849 (2010).
[6] J. L. Davy, "Sound transmission of cavity walls due to structure borne transmission via point and line connections," *J. Acoust. Soc. Am.*, **132**, 814–821 (2012).
[7] A. Arjunana, C. J. Wang, K. Yahiaouia, D. J. Mynors, T. Morgan, V. B. Nguyen and M. English, "Development of a 3D finite element acoustic model to predict the sound reduction index of stud based double-leaf walls," *J. Sound Vib.*, **333**, 6140–6155 (2014).
[8] M. Yairi, K. Sakagami, M. Morimoto, A. Minemura and K. Andow, "Effect of acoustical damping with a porous absorptive layer in the cavity to reduce the structure-borne sound radiation from a double-leaf structure," *Appl. Acoust.*, **64**, 365–384 (2003).
[9] M. Toyoda, M. Tanaka and D. Takahashi, "Reduction of acoustic radiation by perforated board and honeycomb layer systems," *Appl. Acoust.*, **68**, 71–85 (2007).
[10] M. A. Stewart and R. J. M. Craik, "Impact sound transmission through a floating floor on a concrete slab," *Appl. Acoust.*, **59**, 353–372 (2000).
[11] B. Jonas and H. Per, "Prediction model for the impact sound level of lightweight floors," *Acta Acoust.*, **89**, 309–322 (2003).
[12] M. Junger and D. Feit, *Sound, Structures, and Their Interaction* (MIT Press, reprinted by the Acoustical Society of America, 1993), Chap. 8.
[13] M. Heckl and E. J. Rathe, "Relationship between the transmission loss and the impact-noise isolation of floor structures," *J. Acoust. Soc. Am.*, **35**, 1825–1830 (1963).
[14] I. L. Vér, "Relation between the normalized impact sound level and sound transmission loss," *J. Acoust. Soc. Am.*, **50**, 1414–1417 (1971).

[15] M. Yairi, K. Sakagami, K. Nishibara and T. Okuzono, "Relationship between sound radiation from sound-induced and force-excited vibration: Analysis using an infinite elastic plate model," *J. Acoust. Soc. Am.*, **140**, 453–460 (2016).

[16] D. Takahashi, Y. Furue and K. Matsuura, "Vibration and sound transmission of an elastic plate by a spherical sound wave," *J. Acoust. Soc. Jpn.* (*J*), **35**, 314–321 (1979) (in Japanese with English abstract). The sound insulation for spherical wave incidence is analyzed and numerical examples are given. It is shown that the sound reduction index for the spherical wave incidence is lower than that for the plane wave incidence.

[17] M. Yairi, T. Koga, K. Takebayashi and K. Sakagami, "Transmission of a spherical sound wave through a single-leaf wall: Mass law for spherical wave incidence," *Appl. Acoust.*, **75**, 67–71 (2014).

[18] B. Liu, Y. Jiang and D. Chang, "Sound transmission of a spherical sound wave through a finite plate," *J. Sound Vib.*, **410**, 209–216 (2017).

[19] K. Gösele, "Zur Bewertung der Schalldämming von Bauteilen nach Sollkurven," *Acustica*, **15**, 264–270 (1965). For the appraisal of the reduction of impact noise transmitted through ceilings and of the airborne sound damping of walls and ceilings in Germany, the measurements are compared with the theoretical curves in accordance with DIN 52211.

[20] G. Maidanik, "Response of ribbed panels to reverberant acoustic fields," *J. Acoust. Soc. Am.*, **34**, 809–826 (1962).

[21] M. C. Gomperts, "Sound radiation from baffled thin rectangular plates," *Acustica*, **37**, 93–102 (1977).

[22] A. London, "Transmission of reverberant sound through double walls," *J. Acoust. Soc. Am.*, **22**, 270–279 (1959).

[23] M. Kiyama, K. Sakagami, M. Tanigawa and M. Morimoto, "A basic study on acoustic properties of double-leaf membranes," *Appl. Acoust.*, **54**, 239–254 (1998).

[24] D. Takahashi, "Sound transmission through single plates with absorptive facings," *J. Acoust. Soc. Am.*, **83**, 1453–1457 (1987).

[25] H. Kang, J. Ih, J. Kim and H. Kim, "Prediction of sound transmission loss through multilayered panels by using Gaussian distribution of directional incident energy," *J. Acoust. Soc. Am.*, **107**, 1413–1420 (2000).

[26] F. J. Fahy and P. Gardonio, *Sound and Structural Vibration: Radiation, Transmission and Response*, 2nd ed. (Academic Press, Oxford, 2007), Chap. 5.

[27] M. Yairi, K. Sakagami, E. Sakagami, M. Morimoto, A. Minemura and K. Andow, "Sound radiation from a double-leaf elastic plate with a point force excitation: Effect of an interior panel on the structure-borne sound radiation," *Appl. Acoust.*, **63**, 737–757 (2002).

[28] T. Imamura, *Physics and Green's Function*, Mathematical Physics 4 (Iwanami, Tokyo, 2016), Chap. 5 (in Japanese). Green's functions with several kinds of boundaries are introduced and one with parallel boundaries of infinite extent satisfying the Neumann condition is also discussed in detail.

[29] P. M. Morse and H. Feshbach, *Methods of Theoretical Physics Part 1* (McGraw-Hill, 1953), Chap. 13.